Eur. Phys. J. A (2022) 58:226
https://doi.org/10.1140/epja/s10050-022-00881-w

THE EUROPEAN PHYSICAL JOURNAL A

Check for updates

Regular Article - Theoretical Physics

Two particles interacting via a contact interaction on S^2

Dominic Schuh[1,a], **Thomas Luu**[2]

[1] Helmholtz-Institut für Strahlen- und Kernphysik (Theorie), Universität Bonn, 53115 Bonn, Germany
[2] Institut für Kernphysik and Institute for Advanced Simulation, Forschungszentrum Jülich, 54245 Jülich, Germany

Received: 9 August 2022 / Accepted: 2 November 2022 / Published online: 21 November 2022
© The Author(s) 2022
Communicated by Vittorio Somà

Abstract We consider two particles interacting via a contact interaction that are constrained to a sphere, or S^2. We determine their spectrum to arbitrary precision and for arbitrary angular momentum. We show how the non-inertial frame leads to non-trivial solutions for different angular momenta. Our results represent an extension of the finite-volume Lüscher formulas but now to a non-trivial geometry. We apply our results to predict the spectrum of select two-nucleon halo nuclei and compare with experimental results.

1 Introduction

The eigenvalue solutions to two interacting particles is a standard topic introduced to beginning students of quantum mechanics. Typical first examples include two particles interacting via a contact interaction and the Coulombic solutions of oppositely charged particles. These examples serve as a stepping stone to more complicated quantum mechanical *many-body* systems whose solutions are usually *not* known.

Besides serving a great pedagogical introduction to many-body quantum mechanics, the two-body system itself plays an important role in multiple fields of physics. For example, when the particles are placed within a finite cubic volume their eigenvalue solutions satisfy Lüscher's quantization formula [2,23–25]. Lattice Quantum Chromodynamics (LQCD) calculations of composite two-body systems within a finite volume utilize this relation to extract *infinite-volume* interaction parameters between these particles [4,5]. Sometimes the finite-volume is dictated by the experimental setup as opposed to numerical convenience, as is the case with cold-ion traps. Here the confinement of the two particles can be satisfactorily approximated by an external harmonic oscillator well. Again, the energy solutions here [6,26] provide information on the interacting properties of the particles within this confinement, and in particular whether the two particles undergo a Feshbach resonance when their scattering length diverges [19]. As a final example, solutions exist for two interacting particles within a hard spherical wall [22], providing a means for "tuning" interaction parameters for many-nucleon simulations using nuclear lattice effective field theory [1,21].

The examples above refer to systems residing in three spatial dimensions. But in all these cases there are corresponding solutions in both one- and two-dimensions. A tacit assumption here is that the interaction between the two particles only depends on their relative coordinates. When this is the case, and if the geometry allows it, one can readily separate the system into its relative (Jacobi) and center-of-mass (CM) coordinates. This provides a great simplification to the eigenvalue solutions since one can work solely within the inertial frame.

In this paper we consider two particles *confined* to a sphere of arbitrary radius R (i.e. confined to S^2) and that interact via a contact interaction. Though this interaction again only depends on the relative coordinates, the surface S^2 is a *non-inertial* frame that affords no general separation of relative and CM coordinates and as such there is no simplification to the eigenvalue solution.[1] Yet we show how solutions of arbitrary precision to this system can be found. Furthermore, because of the non-inertial frame, we find an infinite tower of solutions depending on the angular momentum L. We view this system as another excellent pedagogical example of two quantum mechanical interacting particles, but this time within a non-inertial frame.

We then apply our formalism to select two-nucleon halo nuclei. This continues our pedagogical theme as it serves two purposes. First, it demonstrates how one uses the low-energy spectrum of physical systems to constrain the interaction parameters of our model. Interestingly, we find our extracted 2-d scattering lengths share similar features to their 3-d analogs. Second, and just as important, it demonstrates

[a] e-mail: schuh@hiskp.uni-bonn.de (corresponding author)

[1] The exception is the case with zero total angular momentum [8].

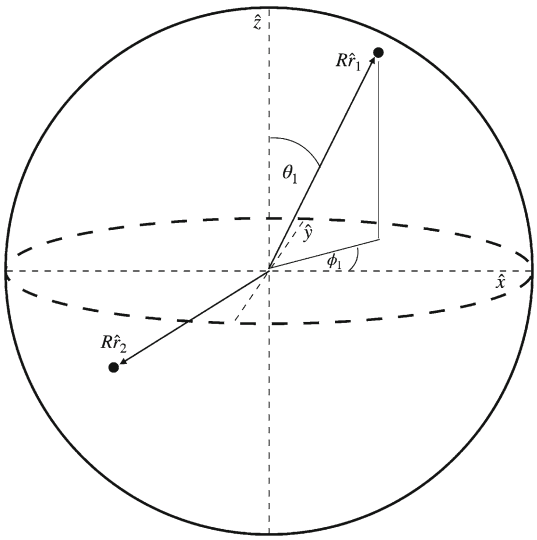


Fig. 1 Two particles confined to the surface of a sphere of radius R. The internal angular coordinates are only shown for the first particle to reduce clutter

the *limitations* of our model. Obviously halo nuclei are complicated many-body systems and approximating such systems with our model is a gross simplification.

Our paper is organized as follows. In Sect. 2 we define our problem. We derive the quantization conditions for arbitrary total angular momentum L in terms of direct summations in Sect. 2.3. When considering explicit values for L, we find analytic expressions for the summations, which we provide for $L = 0$ up to $L = 2$ in Sect. 2.4. We stress, however, that all solutions for $L > 2$ can be readily found using our method. We then apply our results to extract interaction parameters of two-nucleon halo nuclei in Sect. 3. We recapitulate in Sect. 4. Detailed and lengthy derivations are reserved for the appendices.

2 Problem setup

We consider two particles of equal mass m confined to the surface of ball of radius R, as shown in Fig. 1. The particles' positions are then solely dictated by their angles $\hat{r}_1$ and $\hat{r}_2$, which in turn can be expanded in a basis of spherical harmonics $\langle \hat{r}|l, m_l\rangle = Y_{lm_l}(\hat{r})$.

The kinetic term of the Hamiltonian describing such particle movement is well known and is that of a rigid motor,[2]

$$\hat{T}|l, m_l\rangle = \frac{l(l+1)}{2mR^2}|l, m_l\rangle \equiv \epsilon_l|l, m_l\rangle. \tag{1}$$

[2] We set $\hbar = c = 1$ in all our expressions.

2.1 The contact interaction

We assume that the particles interact via a contact interaction only, which in this geometry is given in coordinate space by

$$\begin{aligned}\hat{V}_{12}|\hat{\boldsymbol{r}}_1; \hat{\boldsymbol{r}}_2\rangle &= |\hat{\boldsymbol{r}}_1; \hat{\boldsymbol{r}}_2\rangle \frac{C_0(\Lambda)}{R^2}\delta\left(\hat{\boldsymbol{r}}_1 - \hat{\boldsymbol{r}}_2\right) \\ &= |\hat{\boldsymbol{r}}_1; \hat{\boldsymbol{r}}_2\rangle \frac{C_0(\Lambda)}{R^2}\delta(\cos\theta_1 - \cos\theta_2)\delta(\phi_1 - \phi_2).\end{aligned} \tag{2}$$

Here $C_0(\Lambda)$ is a coefficient that is tuned to reproduce a particular observable of the two-particle system and the variable Λ represents a momentum cutoff scale. The procedure for tuning this coefficient is non-trivial but has been done previously in [3,20], and we only mention some salient features of this procedure relevant to our analysis in Sect. 3. For a more thorough description of this tuning we recommend the reader consult the aforementioned references.

The relevant physical observable is the s-wave scattering length $\tilde{a}$, which in two dimensions is *dimensionless*, despite its name [16]. To a certain degree, the magnitude and sign of this parameter dictates how strongly the particles repulsively or attractively interact with one other. We can define a 'reduced scattering length' a that is *dimensionful* by introducing an arbitrary length scale. We set this length scale to be the radius R of our sphere. The relation between the physical scattering length $\tilde{a}$ (dimensionless) and reduced scattering length a (dimension of length) is given by [16]

$$a = R\ \exp\left(-\frac{\pi}{2\tilde{a}}\right)\ . \tag{3}$$

Note that this definition implies that $a \geq 0$. The tuning of $C_0(\Lambda)$ then follows the procedures described in [3,20]. Assuming a hard-cutoff regulator in momentum space, the coefficient is

$$C_0(\Lambda) = -\frac{2\pi}{m\log(a\Lambda)}\ . \tag{4}$$

We note that though the interaction Eq. (2) is both cutoff and scheme dependent by virtue of the coefficient in Eq. (4), observables are not. We ultimately take the limit $\Lambda \to \infty$ in all our subsequent calculations.

2.2 The integral equation

Our task then is to solve the eigenvalue equation[3]

$$\left(\hat{T}_1 + \hat{T}_2 + \hat{V}_{12}\right)|\psi_{LM}\rangle = E|\psi_{LM}\rangle, \tag{5}$$

where our eigenstates are states with good total angular momentum L and M since our interaction preserves total angular momentum. To do this, we first recast Eq. (5) into

[3] The eigenvalue E includes both rotational and vibrational energies.

integral form,

$$|\psi_{LM}\rangle = \frac{1}{E-\hat{T}_1-\hat{T}_2}\hat{V}_{12}|\psi_{LM}\rangle. \tag{6}$$

We then project the eigenstate onto

$$\langle(l_1l_2)LM| \equiv \sum_{m_1,m_2}\langle l_1,m_1;l_2,m_2|LM\rangle\langle l_1,m_1|\langle l_2,m_2|,$$

where $\langle l_1,m_1;l_2,m_2|LM\rangle$ is a Clebsch–Gordan coefficient. This gives

$$\begin{aligned}\langle(l_1l_2)LM|\psi_{LM}\rangle &= \frac{1}{E-\epsilon_{l_1}-\epsilon_{l_2}}\sum_{l_1'l_2'}\left\langle(l_1l_2)LM|\hat{V}_{12}|(l_1'l_2')LM\right\rangle \\ &\quad\times\langle(l_1'l_2')LM|\psi_{LM}\rangle.\end{aligned} \tag{7}$$

On the RHS above we have inserted the closure relation $\hat{1} = \sum_{l_1'l_2'}|(l_1'l_2')LM\rangle\langle(l_1'l_2')LM|$ and used the fact that $|l_1m_1\rangle$ and $|l_2m_2\rangle$ are eigenstates of $\hat{T}_1$ and $\hat{T}_2$, respectively, with eigenenergies given in Eq. (1).

2.3 Quantization condition for general L

To continue further we require the explicit form of the matrix element $\left\langle(l_1l_2)LM|\hat{V}_{12}|(l_1'l_2')LM\right\rangle$. As this derivation is quite tedious, we leave it for the appendices (Appendix A) and only provide the end result here:

$$\begin{aligned}&\left\langle(l_1l_2)LM|V_{12}|(l_1'l_2')LM\right\rangle \\ &= \begin{cases}\dfrac{C_0(\Lambda)}{R^2}\dfrac{\sqrt{\hat{l}_1\hat{l}_2\hat{l}_1'\hat{l}_2'}}{4\pi}\begin{pmatrix}l_1 & l_2 & L\\ 0&0&0\end{pmatrix}\begin{pmatrix}l_1' & l_2' & L\\ 0&0&0\end{pmatrix}, \\ \qquad \text{if } l_i(l_i+1),\ l_i'(l_i'+1)\le(\Lambda R)^2 \\ 0, \text{ otherwise}\end{cases},\end{aligned} \tag{8}$$

where $\begin{pmatrix}l_1 & l_2 & L\\ m_1 & m_2 & M_L\end{pmatrix}$ is a Wigner 3-j symbol [10] and we define $\hat{l}_i \equiv 2l_i+1$ for brevity. The condition that $l_i(l_i+1)\le(\Lambda R)^2$ and $l_i'(l_i'+1)\le(\Lambda R)^2$ for $i=1,2$ comes from the momentum hard cutoff condition of our interaction. We now plug this expression into Eq. (7), giving

$$\begin{aligned}\langle(l_1l_2)LM|\psi_{LM}\rangle &= \frac{C_0(\Lambda)}{R^2}\frac{\sqrt{\hat{l}_1\hat{l}_2}}{4\pi}\begin{pmatrix}l_1 & l_2 & L\\ 0&0&0\end{pmatrix}\frac{1}{E-\epsilon_{l_1}-\epsilon_{l_2}} \\ &\quad\times\sum_{l_1'l_2'}^{\Lambda R}\sqrt{\hat{l}_1'\hat{l}_2'}\begin{pmatrix}l_1' & l_2' & L\\ 0&0&0\end{pmatrix}\langle(l_1'l_2')LM|\psi_{LM}\rangle.\end{aligned} \tag{9}$$

The equality above holds for all l_i such that $l_i(l_i+1)\le(\Lambda R)^2$ for $i=1,2$. In particular, it holds if we multiply both sides of the equation by $\sqrt{\hat{l}_1\hat{l}_2}\begin{pmatrix}l_1 & l_2 & L\\ 0&0&0\end{pmatrix}$ and then *sum both sides over* l_1 *and* l_2,

$$\begin{aligned}&\sum_{l_1'',l_2''}^{\Lambda R}\sqrt{\hat{l}_1''\hat{l}_2''}\begin{pmatrix}l_1'' & l_2'' & L\\ 0&0&0\end{pmatrix}\langle(l_1''l_2'')LM|\psi_{LM}\rangle \\ &= \frac{C_0(\Lambda)}{4\pi R^2}\sum_{l_1,l_2}^{\Lambda R}\frac{\hat{l}_1\hat{l}_2}{E-\epsilon_{l_1}-\epsilon_{l_2}} \\ &\quad\times\begin{pmatrix}l_1 & l_2 & L\\ 0&0&0\end{pmatrix}^2\sum_{l_1'l_2'}^{\Lambda R}\sqrt{\hat{l}_1'\hat{l}_2'}\begin{pmatrix}l_1' & l_2' & L\\ 0&0&0\end{pmatrix}\langle(l_1'l_2')LM|\psi_{LM}\rangle.\end{aligned} \tag{10}$$

On the LHS above we have introduced new summation indices l_i'' (instead of l_i) to stress that it is the sum that holds under the equality. A trivial solution to the equality occurs if $\langle(l_1l_2)LM|\psi_{LM}\rangle = 0$ for all l_i. To obtain a non-trivial solution, we collect the components $\langle(l_1l_2)LM|\psi_{LM}\rangle$ to one side of the equation,

$$\begin{aligned}0 &= \sum_{l_1'l_2'}^{\Lambda R}\sqrt{\hat{l}_1'\hat{l}_2'}\begin{pmatrix}l_1' & l_2' & L\\ 0&0&0\end{pmatrix}\langle(l_1'l_2')LM|\psi_{LM}\rangle \\ &\quad\times\left[\frac{C_0(\Lambda)}{4\pi R^2}\sum_{l_1,l_2}^{\Lambda R}\frac{\hat{l}_1\hat{l}_2}{E-\epsilon_{l_1}-\epsilon_{l_2}}\begin{pmatrix}l_1 & l_2 & L\\ 0&0&0\end{pmatrix}^2-1\right].\end{aligned} \tag{11}$$

The equality now holds non-trivially if the term in square brackets vanishes. Using the exact form of $C_0(\Lambda)$ from Eq. (4) and equating the term in square brackets to zero gives the desired quantization condition for arbitrary total angular momentum L:

$$\begin{aligned}\log\left(\frac{a}{R}\right) &= \sum_{l_1,l_2}^{\Lambda R}\frac{(2l_1+1)(2l_2+1)}{l_1(l_1+1)+l_2(l_2+1)-x}\begin{pmatrix}l_1 & l_2 & L\\ 0&0&0\end{pmatrix}^2 \\ &\quad-\log(\Lambda R)\,,\end{aligned} \tag{12}$$

where $x \equiv 2mER^2$. The summation above is over all l_i such that $l_i(l_i+1)\le(\Lambda R)^2$.

The eigenvalues E, or equivalently x, of Eq. (5) are those that satisfy the equality in Eq. (12). This represents Lüscher's formula on S^2 for each rotational band L under the assumption of a pure contact interaction.

2.4 Closed expressions for select L

When we concentrate on specific values of L and take the limit $\Lambda\to\infty$ we can further simplify Eq. (12) and obtain closed expressions. We do this explicitly for $L=0$ and 1, and provide the closed expression for $L=2$ without derivation. In principle it is possible to obtain closed expressions for

concrete values of $L > 2$, but the derivation becomes much more tedious and onerous.

2.4.1 $L = 0$

To start, note that the sums over l_1 and l_2 in Eq. (12) are restricted by the triangle inequalities of the Wigner 3-j symbol

$$|l_1 - l_2| \leq L \leq l_1 + l_2 \,. \tag{13}$$

For $L = 0$ this implies that $l_1 = l_2 \equiv l$. The 3-j symbol simplifies to $\frac{(-1)^l}{\sqrt{2l+1}}$ and Eq. (12) becomes

$$\log\left(\frac{a}{R}\right) = \lim_{\Lambda\to\infty} \sum_{l}^{\Lambda R} \frac{2l+1}{2l(l+1)-x} - \log(\Lambda R) \tag{14}$$

If we identify the cutoff with some maximum angular momentum λ via $\lambda(\lambda+1) \equiv (\Lambda R)^2$, then our expression above can be written as

$$\log\left(\frac{a}{R}\right) = \lim_{\lambda\to\infty} \sum_{l}^{\lambda} \frac{2l+1}{2l(l+1)-x} - \frac{1}{2}\log(\lambda(\lambda+1)) \tag{15}$$

The sum can be explicitly expressed in terms of the digamma function $\psi(x) = \frac{\mathrm{d}}{\mathrm{d}x}\log(\Gamma(x))$,

$$\begin{aligned}\sum_{l}^{\lambda} \frac{2l+1}{2l(l+1)-x} &= \frac{1}{2}\Bigg(\psi\left(\lambda - \frac{1}{2}\sqrt{2x+1} + \frac{3}{2}\right) \\ &+\psi\left(\lambda + \frac{1}{2}\sqrt{2x+1} + \frac{3}{2}\right) - \psi\left(\frac{1}{2}\left(1 - \sqrt{2x+1}\right)\right) \\ &-\psi\left(\frac{1}{2}\left(1 + \sqrt{2x+1}\right)\right)\Bigg) \,. \end{aligned} \tag{16}$$

In the limit $\lambda \to \infty$ the first two terms on the RHS above exactly cancel the logarithm term in Eq. (15) What remains gives us our closed-form expression,

$$\begin{aligned}\log\left(\frac{a}{R}\right) = -\frac{1}{2}\Bigg[&\psi\left(\frac{1}{2}\left(1 - \sqrt{2x+1}\right)\right) \\ &+\psi\left(\frac{1}{2}\left(1 + \sqrt{2x+1}\right)\right)\Bigg] \equiv Z_0(x) \,. \end{aligned} \tag{17}$$

2.4.2 $L = 1$

The triangle inequality in this case requires that, given $l_1 \equiv l$, the sum over l_2 is restricted to the values $|l-1|$, l, and $l+1$. However, the 3-j symbol vanishes for $l_1 = l_2 = l$ (when $L = 1$), and so Eq. (12) becomes the sum over two expressions only,

$$\begin{aligned}\log\left(\frac{a}{R}\right) = \frac{3}{2-x}\begin{pmatrix} 0 & 1 & 1 \\ 0 & 0 & 0 \end{pmatrix}^2 + \sum_{l\geq 1}^{\Lambda R}\Bigg(&\frac{4l^2-1}{2l^2-x}\begin{pmatrix} l & l-1 & 1 \\ 0 & 0 & 0 \end{pmatrix}^2 \\ &+\frac{(2l+1)(2l+3)}{2(l+1)^2-x}\begin{pmatrix} l & l+1 & 1 \\ 0 & 0 & 0 \end{pmatrix}^2\Bigg) - \log(\Lambda R) \,. \end{aligned} \tag{18}$$

The first term on the RHS above comes from the $l = 0$ contribution. After simplifying the 3-j symbols the sums can be performed and analytically expressed in terms of digamma functions. The $\Lambda \to \infty$ limit can be subsequently taken, giving

$$\begin{aligned}\log\left(\frac{a}{R}\right) &= -\frac{1}{2}\left[\psi\left(1 - \sqrt{\frac{x}{2}}\right) + \psi\left(1 + \sqrt{\frac{x}{2}}\right)\right] \\ &\equiv Z_1(x) \,. \end{aligned} \tag{19}$$

The fact that there exists a non-trivial quantization condition for $L = 1$, despite the interaction being a pure contact interaction, comes from the fact that our general expression in Eq. (12) is derived using single-particle coordinates as opposed to relative coordinates.

2.4.3 $L = 2$

The steps used for the $L = 0, 1$ cases can be analogously applied to $L = 2$ (and higher). Clearly the sum over l_2 for a given l_1 becomes more involved as L becomes larger, and as such, the expressions become more complicated and cumbersome to express. Therefore we do not show these steps here but instead provide the expression for $L = 2$ without derivation:

$$\begin{aligned}\log\left(\frac{a}{R}\right) = \frac{1}{12-8x}\Bigg[&2 + 3(x-2)\Bigg\{\psi\left(\frac{1}{2}\left(3 - \sqrt{-3+2x}\right)\right) \\ &+\psi\left(\frac{1}{2}\left(3 + \sqrt{-3+2x}\right)\right)\Bigg\} + x\Bigg\{\psi\left(\frac{1}{2}\left(1 - \sqrt{1+2x}\right)\right) \\ &+\psi\left(\frac{1}{2}\left(1 + \sqrt{1+2x}\right)\right)\Bigg\}\Bigg] \equiv Z_2(x) \,. \end{aligned} \tag{20}$$

2.5 Limits and zeros of the quantization relations for $L = 0, 1$ cases

The structure of these quantization equations for energies $x \in \{-9, 40\}$ is displayed in Fig. 2. These will be utilized to find solutions to the Schrödinger equation for two particles on a sphere in the following chapter. One may notice the divergent parts of each graph, which corresponds to the case of no interaction.

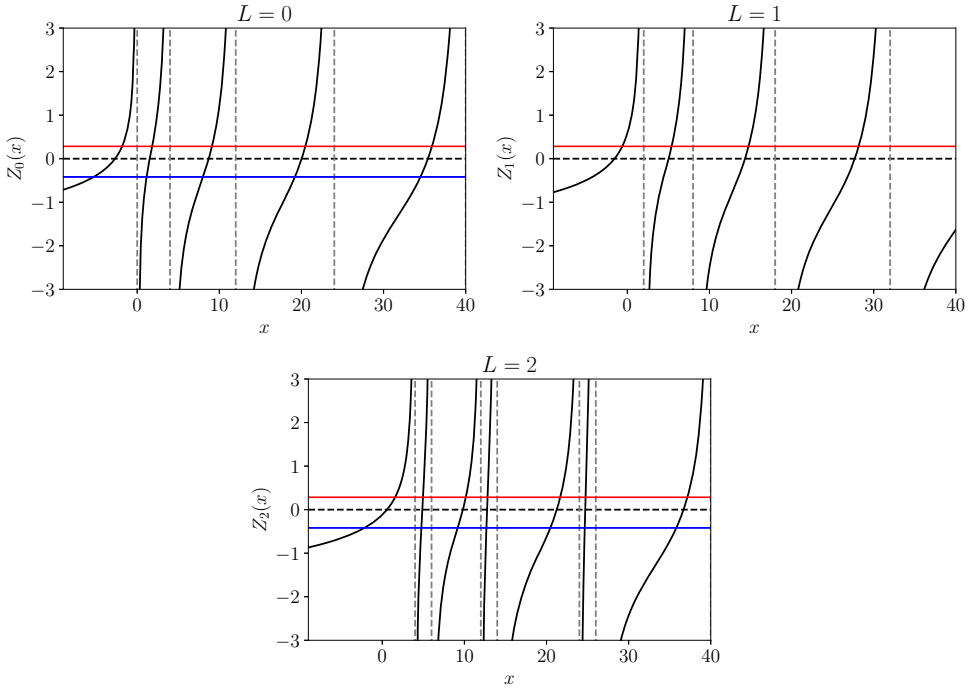


Fig. 2 Quantization curves for the three lowest angular momenta L given by Eqs. (17), (19), and (20). The vertical dashed lines correspond to the non-interacting energies. The horizontal red line is the experimentally determined value of $-\frac{\pi}{2\tilde{a}}$ in the spin-singlet ($S = 0$) case, while the blue line corresponds to the spin-triplet ($S = 1$) case, both of which are described and used in Sect. 3

As already mentioned earlier, in two dimensions the scattering length $a \geq 0$ [27]. In the limit $a \gg R$, the solutions to Eq. (17) approach the non-interacting energies from below. In the limit $a \ll R$ we have, in addition to the deeply bound solution $x \to -\infty$ (i.e. the so-called "dimer solution"), solutions that also approach the non-interacting energies, but now from above. We can expand the solutions x about the non-interacting energies by considering the limit $|\log(a/R)| \gg 1$. For the nth solution, where $n \in \mathbb{Z}_{\geq 0}$, we find for the $L = 0$ case

$$x = 2n(n+1) - \frac{2n+1}{\log(a/R)} + \mathcal{O}\left(\log(a/R)^{-2}\right) . \tag{21}$$

This expression is valid for both limits $a \to \infty$ and $a \to 0$ (keeping R fixed). The bound dimer solution valid as $a \to 0$ scales as

$$x = -\frac{2R^2}{a^2} + \mathcal{O}(a^2) . \tag{22}$$

Given that $x = 2mER^2$, this corresponds to the standard dimer binding energy $E = -\frac{1}{ma^2}$. Similarly, for $L = 1$ we have

$$x = 2(n+1)^2 - \frac{2(n+1)}{\log(a/R)} + \mathcal{O}\left(\log(a/R)^{-2}\right) , \tag{23}$$

which is again valid for both limits $a \to \infty$ and $a \to 0$ while keeping R fixed. The dimer solution scales identically the same as the $L = 0$ case, Eq. (22).

Another interesting limit is to consider the case when $a/R = 1$, corresponding to the $|\tilde{a}| \to \infty$ limit.[4] Solutions to Eq. (12) in this case occur when the curves in Fig. 2 intersect the x-axis, corresponding to zeros of the quantization equations. We provide these zeros to machine precision for $L = 0$, 1, and 2 in Table 1. For both $L = 0$ and $L = 1$ there exists an $x_0 < 0$ solution corresponding to a bound state in this limit.

The behavior of the eigenvalue solutions near a general zero x_0 when $a \approx R$ for the $L = 0$ band is

$$x = x_0 + \frac{4\sqrt{2x_0+1}\log(a/R)}{\psi^{(1)}\left(\frac{1}{2} - \frac{1}{2}\sqrt{2x_0+1}\right) - \psi^{(1)}\left(\frac{1}{2} + \frac{1}{2}\sqrt{2x_0+1}\right)} + \mathcal{O}\left(\log(a/R)^2\right) , \tag{24}$$

while for $L = 1$ it is

$$x = x_0 + \frac{4\sqrt{2x_0}\log(a/R)}{\psi^{(1)}\left(1 - \sqrt{\frac{x_0}{2}}\right) - \psi^{(1)}\left(1 + \sqrt{\frac{x_0}{2}}\right)} + \mathcal{O}\left(\log(a/R)^2\right) , \tag{25}$$

[4] If both $a \to \infty$ and $R \to \infty$, while $a/R = 1$, then this corresponds to the 2-d unitary limit where all length scales have been "integrated out".

Table 1 Zeros x_0 for the three lowest rotational bands

$L=0$	$L=1$	$L=2$
−2.69519416311127(1)	−1.56227783993538(1)	0.57785048142503(1)
1.53660948605491(1)	5.02284537252901(1)	4.86959138770876(1)
8.70562260382481(1)	14.32769206430169(1)	12.76394742135846(1)
20.02549569293160(1)	27.692061960724 71(1)	21.24994781781113(1)
⋮	⋮	⋮

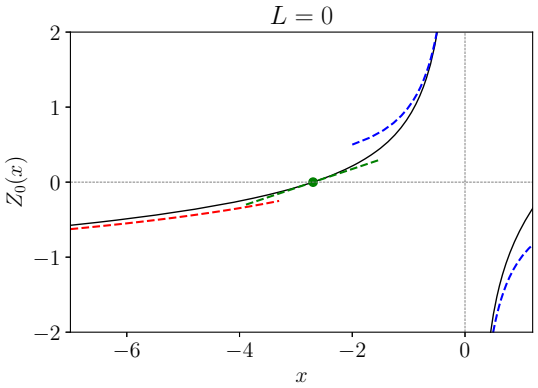


Fig. 3 The limits of the quantization equation for the $L=0$ case. The red dashed curve corresponds to Eq. (22), the blue dashed line Eq. (21), and the green dashed curve Eq. (24) using $x_0=-2.69519$. The solid black line is given by Eq. (17)

where $\psi^{(1)}(z)\equiv\frac{d}{dz}\psi(z)$. In Fig. 3 we plot these limiting expressions and compare them to the exact solution for the $L=0$ case.

2.6 Comparison with $S^1\times S^1$ topology and 2-D harmonic oscillator

As mentioned earlier, the quantization condition for two particles interacting in a confined space has been determined in other 2-D systems. Here we take the opportunity to compare our $L=0$ result Eq. (17) with its analog in the $S^1\times S^1$ geometry and the harmonic oscillator.

Busch et al. [6] have derived the case for the 2-D harmonic oscillator with frequency ω,

$$\log\left(\frac{a}{b}\right)=-\frac{1}{2}\psi\left(\frac{1}{2}-\frac{x}{2}\right)\,, \tag{26}$$

where $x=E/\omega$ with E the eigenenergy and $b=1/\sqrt{2m\omega}$ is the oscillator parameter.

For a 2-D square lattice of side L with periodic boundary conditions (i.e. the torus or $S^1\times S^1$ topology), a thorough derivation is provided in [3], giving

$$\begin{aligned}\frac{2}{\pi}\log\left(2\pi\frac{a}{L}\right)&=\lim_{\Lambda\to\infty}\frac{1}{\pi^2}\sum_{\boldsymbol{n}}^{|\boldsymbol{n}|\le\Lambda}\frac{1}{\boldsymbol{n}^2-x}-\frac{2}{\pi}\log(\Lambda)\\&\equiv\frac{1}{\pi^2}S_2(x)\,.\end{aligned} \tag{27}$$

Here $S_2(x)$ is the two dimensional zeta function, $\boldsymbol{n}=(n_i,n_j)\in\mathbb{Z}^2$, and $x=mEL^2/(4\pi^2)$.

The dependence of these functions on x is shown Fig. 4, and should be compared with the top panel of Fig. 2. In all cases, the curves approach their respective non-interacting solutions in both limits $a\to\infty$ and $a\to 0$, all other parameters held fixed. Furthermore, all cases have $x_0<0$ as the lowest x-axis intercept, corresponding to a bound state in the limit $a/R=a/b=2\pi a/L=1$.

Because the harmonic oscillator and torus results are derived in geometries in which the CM and relative coordinates are exactly separable, it is trivial to determine their quantization conditions for *non-zero CM motion*. Such motion corresponds to a quantized CM energy E_{CM}, which in dimensionless units is $x_{CM}=E_{CM}/\omega$ for the harmonic oscillator and $x_{CM}=mE_{CM}L^2/(4\pi^2)$ for the torus. To obtain the quantization curves for these cases, one shifts the curves in Fig. 4 to the right by exactly x_{CM}. In this manner any non-zero CM quantization curve in the harmonic oscillator and torus cases can be obtained directly from the curves shown in Fig. 4.

For S^2 there is no trivial connection to the lowest energy quantization curve given by $L=0$, since the geometry is not amenable to CM and relative motion separability. The analog of different CM motion manifests itself as different rotational bands L, and as can be seen from Fig. 2 the $L=1$ and $L=2$ curves (and in general $L>2$) are not connected to $L=0$ by any constant shift in the x-axis.

3 Application: predicting energy levels of two-nucleon halo nuclei

Halo nuclei consist of a tightly bound core of nucleons surrounded by a small group of loosely bound, or halo, nucleons. The resulting nuclei appear much larger than the radius of the original tightly bound core. A classic example is the ^{11}Li halo nucleus originally found by Tanihata et al. [30]. This nucleus can be decomposed into a three-body system, ^{9}Li + 2n, where the ^{9}Li constitutes the tightly bound core and the two neutrons the halo nucleons that are considered to be loosely bound and interacting. Another example is ^{6}He,

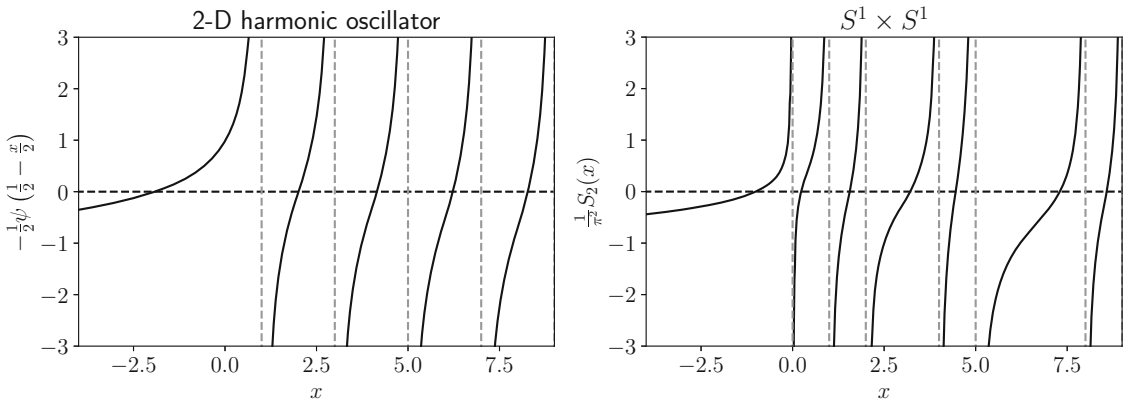


Fig. 4 S-wave quantization conditions for the 2-D harmonic oscillator (left, Eq. (26)) and the $S^1 \times S^1$ topology (right, Eq. (27)). The vertical dashed gray lines correspond to the non-interacting energies of each system. Compare with the $L = 0$ quantization relation on S^2 (top panel of Fig. 2 and Eq. (17))

which can also be decomposed into a tightly bound core, ^{4}He, plus two halo neutrons, again loosely bound and interacting. Both of these systems are only stable[5] as a three-body constellation, and therefore are considered *borromean* [32].

A simple, albeit crude, approximation to these systems is to assume that the two nucleons are constrained to interact on a sphere with halo radius R and that the core is located at the center of this sphere. The confinement of the halo nucleons is assumed to be due to some non-trivial interaction with the core, which we approximate as infinitely massive and therefore non-dynamical.[6] When the core has its own angular quantum numbers, we may couple the angular momentum of the halo nucleons with that of its core, but aside from that, the core has no other influence on the halo nucleons. If we further assume that the interaction between the nucleons is contact in nature,[7] then our formalism of the previous section directly describes this situation.[8] Under this approximation radial excitations are not possible and therefore there are only vibrational excitations for each rotational band. Thus our model cannot capture all relevant dynamics of halo nuclei, since they will have both radial and vibrational modes.

Nucleons are of course fermions with spin and isospin equal to 1/2. To incorporate our results from the previous section, we must take the nucleons' spins, isospins, and their Pauli-exclusion into account. For the two nucleons to 'feel' the s-wave interaction, we must couple their spins and isospins to total spin and isospin $S = 0, T = 1$ (e.g. 'spin-singlet' two-neutron system) or $S = 1, T = 0$ (i.e. 'spin-triplet' deuteron system), respectively. We then couple their total spin S and angular momentum L to make total angular momentum J_{NN}. An anti-symmetric two-nucleon wavefunction requires

$$L + S + T - l_1 - l_2 = \text{odd} \,,$$

and this in turn restricts the allowed angular momentum L of the two nucleons. The total angular momentum J_{NN} of the halo nucleons is then coupled with the angular momentum of the core to obtain the total angular momentum of the halo system J. Finally, the parity of the two-nucleon system is $(-1)^L$, and is multiplied with the parity of the core to obtain the overall parity π of the halo system.

Before we can use our formalism to predict energy levels, however, we have to tune the parameters (i.e. $\tilde{a}$ or equivalently a/R) of our theory. Such tuning is a common procedure in any low-energy effective theory, and in what follows we describe in detail how we use the low-energy spectrum of the ^{6}He and ^{11}Li halo nuclei to determine these parameters. In particular, these systems will allow us to determine the spin-singlet scattering length $\tilde{a}_0$. We also consider the ^{6}Li system which will allow us to determine the spin-triplet scattering length $\tilde{a}_1$.

3.1 Helium-6

Here we have two neutrons surrounding a ^{4}He core. The two neutrons are thus in the $S = 0, T = 1$ channel. The three lowest allowed angular momentum bands are $L = 0$, $L = 1$, and $L = 2$, with $L = 1$ being odd in parity and the others even. As the ^{4}He core has $J_{\text{C}}^{\pi_{\text{C}}} = 0^+$ angular momentum, the total angular momenta of the halo nucleus for these bands are simply $J^\pi = J_{\text{NN}}^\pi = 0^+,\ 1^-$, and 2^+. Within our approximation the interaction of two neutrons on a 2d surface is described

[5] Stable in this context applies only to the strong interaction.

[6] Such an approximation has been used to describe doubly-excited atomic electrons interacting via a contact interaction [11,12] and via a modified coulomb interaction [28], for example.

[7] Such an approximation is only valid at energies well below the pion mass [15].

[8] Naturally there exist more sophisticated models and calculations of these systems, see e.g. Refs. [7,14,17] and references within.

solely by the parameter $\tilde{a}_0$, where we add the subscript 0 to denote that this parameter is for the spin-singlet $S = 0$ system. This parameter is *independent* of the halo nucleus. As it is also dimensionless, a single empirical (dimensionful) energy is not sufficient to constrain this parameter and therefore a second energy is required. We use the experimental $J^\pi = 0^+$ and 2^+ energies of the ^{6}He halo nucleus [13,31], measured relative to the $^4\text{He} + n + n$ threshold, to constrain the dimensionful parameters a_0 and R of our theory, which we stress are halo nucleus *dependent*. We then obtain $\tilde{a}_0$ by the relation Eq. (3). We find

$$\tilde{a}_0 = -5.58(6)\ . \tag{28}$$

The experimental energies used to obtain this value, as well as the resulting a_0, R, and predicted energy levels of our model for the $J^\pi = 0^+,\ 1^-$ and 2^+ rotational bands, are given in Fig. 5. We take the mass of the neutron as $m = 939.565$ MeV.

To obtain the errors of the fit parameters quoted in Fig. 5, we first assume that the experimental errors for the $J = 0$ and $J = 2$ energies are uncorrelated and follow a normal distribution with width dictated by their respective errors. We then sample these energies from their distributions, each time performing our fit to obtain a_0, R, and $\tilde{a}_0$, and we tally these results. The mean of these tallies is our quoted values of these terms in Fig. 5, and the standard deviation their errors. Our sample size is 10,000.

The determined value of $\tilde{a}_0$ then fixes $\log(a_0/R)$ through the relation Eq. (3), which we show as the red line in the $L = 0,\ 1$ and 2 plots in Fig. 2. The intercept of this red line with the solid black curves in these plots gives us our energy solutions. Our fitting procedure is guaranteed to reproduce the lowest 0^+ and 2^+ experimental energies and their errors, as these were used to obtain our fit parameters. The higher intercepts then provide our predicted energy levels shown in Fig. 5.

As already mentioned above, the applicability of our model is quite limited due to its extreme simplicity, and this is quite obvious when looking at its predicted $J^\pi = 1^-$ energies. Our model predicts as its lowest state a *negative* energy solution, although experimentally no such state exists. Furthermore, there exist positive energy solutions that are predicted in other rotational bands that have no obvious experimental counterparts. It is also interesting to compare our estimate of the halo radius $R = 6.258(15)$ fm which is nearly a factor of two larger than the experimental result of $R_{\text{exp}} = 3.08(10)$ fm [9]. Again, this disagreement is not surprising given the level of crudeness of our model.

3.2 Lithium-11

The ^{9}Li core has angular quantum numbers $3/2^-$, and for the ^{11}Li halo system there is only the measured $J = 3/2^-$ ground state energy $E_0 = -0.369$MeV [18,29] that has definitive quantum numbers assigned. However, given that we determined $\tilde{a}_0$ in the previous section (which in our approximation is independent of halo nucleus), we have sufficient information to determine a_0 and R for this system. In this case we tally fit results obtained from uncorrelated samplings of E_0 and $\tilde{a}_0$ to arrive at a_0 and R, and then subsequently predict the higher energy levels. Our results are given in the right panel of Fig. 5. When coupling the angular momentum J_{NN} of the halo nucleons with that of the $3/2^-$ core, our model predicts multiplets of energies in the $L = 1$ and $L = 2$ cases. We label these multiplets in our figure.

As in the ^{6}He case, our model predicts another negative energy solution near threshold coming from the $L = 1$ case, which is not seen experimentally. Our model again predicts many positive energy solutions that have no obvious experimental counterparts. Our estimate of the halo radius $R = 10.154(24)$fm deviates from its experimental value, $R_{\text{exp}} = 6.5(3)$fm [9]. Again, this level of disagreement is not surprising given the simplicity of our model.

3.3 Lithium-6

Though not technically considered a halo nucleus, the small separation energy for $^4\text{He}+n+p$ breakup (small compared to the binding energy of its ^{4}He core) suggests that the nucleus is extended in size. We therefore assume that the ^{4}He acts as the core and the 'halo' nucleons for this system consist of a neutron and proton. This system supports both $S = 0,\ T = 1$ and $S = 1,\ T = 0$ channels, therefore we expect the spectrum to be much richer than in the previous two examples. Both of these channels can couple to $L = 0$ and 2 angular momenta for positive parity. The $S = 0,\ T = 1$ channel can also couple with the negative parity $L = 1$ angular momentum. When coupled with $J_C^{\pi_C} = 0^+$ of the core, we have $J^\pi(T) = 1^+(0),\ 2^+(0),\ 3^+(0),\ 0^+(1),\ 2^+(1)$, and $1^-(1)$ as possible quantum numbers. We use $m = 2\mu = 938.918$ MeV, where μ is the reduced mass of the proton and neutron.

We assume isospin charge symmetry, meaning that the (dimensionless) scattering length in the spin-singlet $S = 0$ channel is the same as that determined in the ^{6}He case given in Eq. (28). To determine the spin-triplet $S = 1$ scattering length, we again use the two lowest experimental energies [31] of this system, measured relative to the $^4\text{He} + n + p$ breakup threshold. Here the two lowest energies have the quantum numbers 1^+ and 3^+ states. We find

$$\tilde{a}_1 = 3.760(7)\ , \tag{29}$$

where the subscript 1 denotes the $S = 1$ spin-triplet system. Note the change of the sign compared to the spin-singlet case

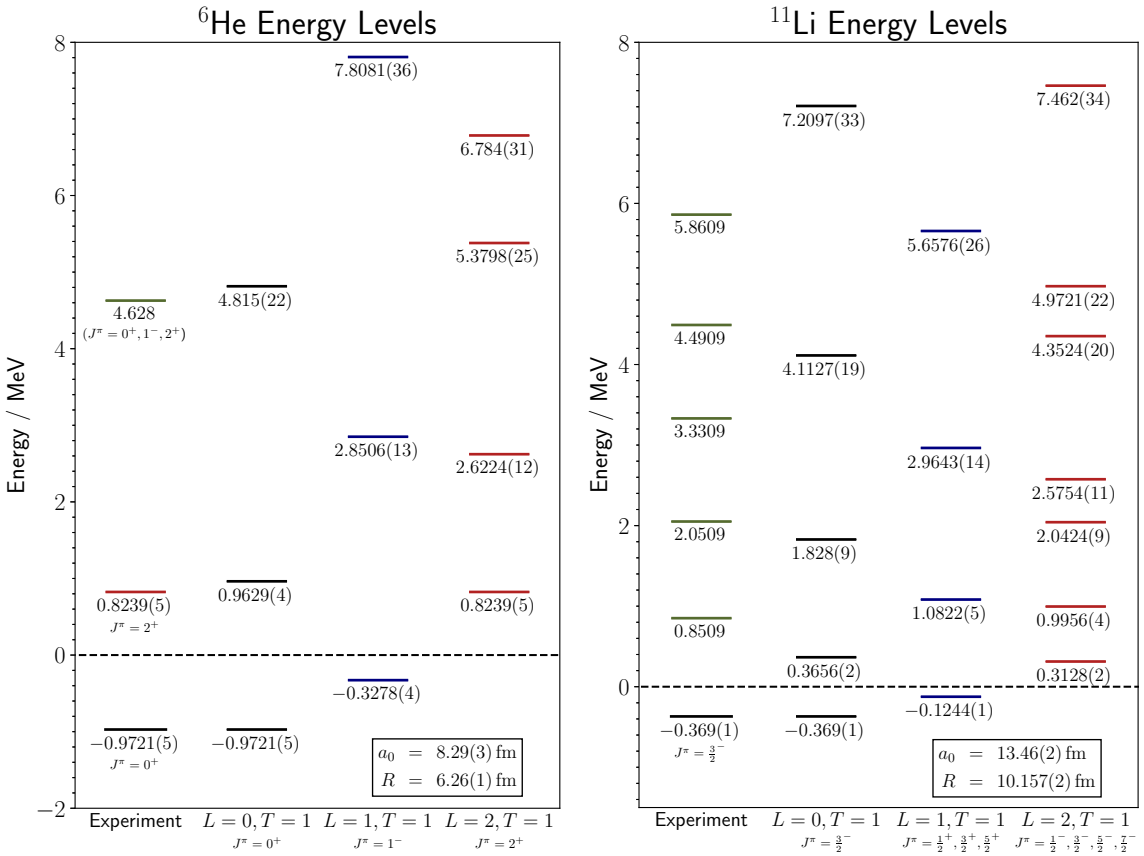


Fig. 5 Two-neutron halo energy levels for select rotational bands of ^{6}He (left) and ^{11}Li (right), compared to experiment. The lowest two experimental energies of ^{6}He and the lowest experimental energy of ^{11}Li were used to determine $\tilde{a}_0$ and our model parameters shown in the boxed insets. These were then used to make the predictions of the energy levels. Where possible we have provided the J^π quantum numbers of the levels, and color-coded the levels to match the quantum numbers. The uncertainties do not represent widths of the levels, but rather are the uncertainties of our model predictions, given the level of accuracy of the experiments

in Eq. (28).[9] As before, the determined value of $\tilde{a}_1$, along with the experimental energies, fixes $\log(a_1/R)$ through the relation Eq. (3). We show this result as the blue line in the $L = 0$ and 2 plots in Fig. 2. The intersection of this blue line with the black curves gives us our predicted energy levels. The experimental energies, our determined a_0, a_1 and R parameters for this system, as well as our predicted energy levels are shown in Fig. 6.

It is interesting to note that relative to the $^4\text{He} + n + p$ breakup threshold, the ^{6}Li system has three positive parity negative energy states. The two lowest energies, both in the $T = 0$ channel, are exactly captured in our model, since we use these energies to fit our parameters $\tilde{a}_1$ and the combination a_1 and R. But our model also predicts a third positive parity negative energy corresponding to the $T = 1$ channel. This is due to the spin-singlet scattering length $\tilde{a}_0$ and the energy of this state coincides with the intersection of the red line with the lowest black curve of $L = 0$ in Fig. 2. The correct ordering of these levels is captured in our model, however the experimental value of this state is much closer to the $^4\text{He} + n + p$ threshold, while our prediction is significantly lower in energy. Lastly, our model predicts a near threshold negative energy in the negative parity $J^\pi(T) = 1^-(1)$ band due to the coupling with $L = 1$, which is not observed experimentally.

[9] A similar sign change occurs for the two-nucleon scattering lengths in *three* dimensions.

4 Conclusion

In this paper we derived the quantization condition for two-particles constrained to a sphere, or S^2, and under the assumption that they interact via a contact interaction. We show how the energy levels of the system are related to the reduced scattering length a and radius of the sphere R. As the constraint on S^2 represents a non-inertial frame, the system is not amenable to a separation of CM and relative coordinates. As such, there is an infinite tower of solutions for each total

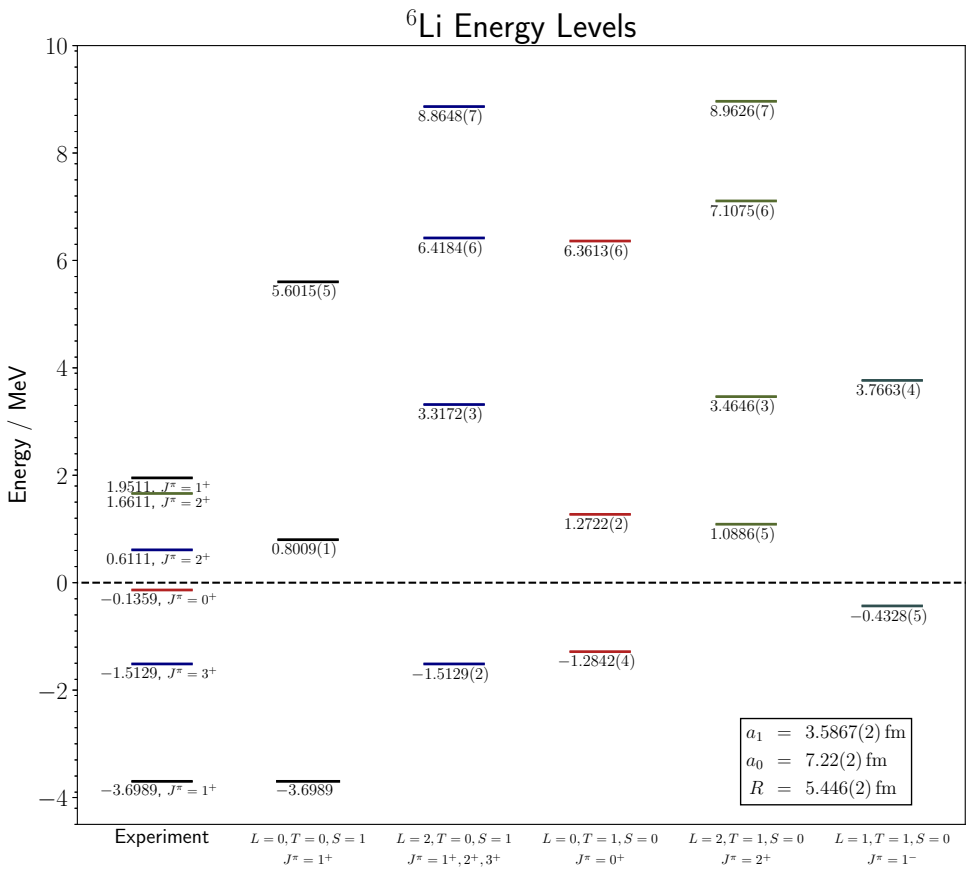


Fig. 6 Two-nucleon halo energy levels for select rotational bands of ^{6}Li and comparison with experimental values, where available [31]. The lowest two experimental energies are used to determine the parameters of our model, which are shown in the boxed inset. Where possible we have provided the J^π quantum numbers of the levels, and color-coded the levels to match the quantum numbers. The uncertainties do not represent widths of the levels, but rather are the uncertainties of our model predictions

angular momentum L, each of which is different and *not* related by any constant offset from each other. We provide a solution for any L in terms of a general sum, but for the $L = 0$, 1, and 2 cases we obtain closed form expressions. We also derive expressions in the limit $a \gg R$, $a \ll R$, and $a \to R$.

We then applied our formalism to select two-nucleon halo nuclei under the assumption that the halo nucleons are confined to a sphere of halo radius R and the core is infinitely massive and therefore non-dynamical. We tuned our system-dependent parameters to the low-lying spectrum of these halo nuclei and determined the spin-singlet $S = 0$ and spin-triplet $S = 1$ scattering lengths. We then used these results to predict the higher-lying spectrum. Our results for the halo radius disagreed by up to a factor of two from experiment, but given the level of crudeness of our approximation this was not a surprising result. Despite such disagreements, our application to halo nuclei provides an example of how one tunes the parameters of an effective theory using empirical data, while at the same time demonstrating the limitations of our particular theory.

One might consider improving our formalism by expanding beyond a simple contact interaction to include derivative, or momentum-dependent contact terms, similar to what was done, for example, in [2]. Here the 'curvature' of the surface may complicate such an investigation, but to what degree is unknown.

Finally, our formalism and its application to two-nucleon halo nuclei, provides another excellent pedagogical example of two quantum mechanical interacting particles, but this time within a non-inertial frame.

Acknowledgements We thank Christoph Hanhart for getting us started on this project, and Evan Berkowitz, Johann Ostmeyer, and Ulf Meißner for their critical reading of the manuscript. We are also immensely indebted to Andreas Nogga for his insightful comments. This work was supported in part by the NSFC and the Deutsche Forschungsgemeinschaft (DFG, German Research Foundation) through the funds provided to the Sino-German Collaborative Research Center TRR110 "Symmetries and the Emergence of Structure in QCD" (NSFC Grant No. 12070131001, DFG Project-ID 196253076 - TRR 110).

Funding Information Open Access funding enabled and organized by Projekt DEAL.

Data Availability Statement This manuscript has no associated data or the data will not be deposited. [Authors' comment: The data has been produced via results stated in the paper. Explicit values may be obtained via direct correspondence with either of the authors.]

Open Access This article is licensed under a Creative Commons Attribution 4.0 International License, which permits use, sharing, adaptation, distribution and reproduction in any medium or format, as long as you give appropriate credit to the original author(s) and the source, provide a link to the Creative Commons licence, and indicate if changes

were made. The images or other third party material in this article are included in the article's Creative Commons licence, unless indicated otherwise in a credit line to the material. If material is not included in the article's Creative Commons licence and your intended use is not permitted by statutory regulation or exceeds the permitted use, you will need to obtain permission directly from the copyright holder. To view a copy of this licence, visit http://creativecommons.org/licenses/by/4.0/.

A Derivation of $\left\langle (l_1 l_2) LM | \hat{V}_{12} | (l_1' l_2') LM \right\rangle$

In Eq. (8) we stated the result of the matrix element

$$\left\langle (l_1 l_2) LM | \hat{V}_{12} | (l_1' l_2') LM \right\rangle$$

which we will now go over in more detail. We start by inserting two complete sets of position eigenstates in order to evaluate the potential $\hat{V}_{12}$ in coordinate space and furthermore make use spherical harmonics.

$$\begin{aligned}
&\langle l_1 m_1; l_2 m_2 | \hat{V}_{12} | \lambda_1 \mu_1; \lambda_2 \mu_2 \rangle \\
&= \frac{C_0(\Lambda)}{R^2} \int d\hat{\boldsymbol{r}}_1 d\hat{\boldsymbol{r}}_2 \langle l_1 m_1; l_2 m_2 | \hat{\boldsymbol{r}}_1; \hat{\boldsymbol{r}}_2 \rangle \delta\left(\hat{\boldsymbol{r}}_1 - \hat{\boldsymbol{r}}_2\right) \\
&\quad \times \langle \hat{\boldsymbol{r}}_1; \hat{\boldsymbol{r}}_2 | \lambda_1 \mu_1; \lambda_2 \mu_2 \rangle \\
&= \frac{C_0(\Lambda)}{R^2} \int d\hat{\boldsymbol{r}}_1 Y^*_{l_1 m_1}(\hat{\boldsymbol{r}}_1) Y^*_{l_2 m_2}(\hat{\boldsymbol{r}}_1) Y_{\lambda_1 \mu_1}(\hat{\boldsymbol{r}}_1) Y_{\lambda_2 \mu_2}(\hat{\boldsymbol{r}}_1) \,.
\end{aligned} \tag{30}$$

Usage of straightforward spherical harmonics algebra leads to the following expression:

$$\begin{aligned}
&\int d\hat{\boldsymbol{r}}\; Y^*_{l_1 m_1}(\hat{\boldsymbol{r}}) Y^*_{l_2 m_2}(\hat{\boldsymbol{r}}) Y_{\lambda_1 \mu_1}(\hat{\boldsymbol{r}}) Y_{\lambda_2 \mu_2}(\hat{\boldsymbol{r}}) \\
&= \frac{\sqrt{(2l_1+1)(2l_2+1))(2\lambda_1+1)(2\lambda_2+1)}}{4\pi} \\
&\quad \times \sum_{LM} (2L+1) \begin{pmatrix} l_1 & l_2 & L \\ -m_1 & -m_2 & M \end{pmatrix} \begin{pmatrix} L & \lambda_1 & \lambda_2 \\ -M & \mu_1 & \mu_2 \end{pmatrix} \\
&\quad \times \begin{pmatrix} l_1 & l_2 & L \\ 0 & 0 & 0 \end{pmatrix} \begin{pmatrix} L & \lambda_1 & \lambda_2 \\ 0 & 0 & 0 \end{pmatrix} \\
&\equiv \mathscr{Y}_4(l_1, m_1, l_2, m_2, \lambda_1, \mu_1, \lambda_2, \mu_2) \,.
\end{aligned} \tag{31}$$

The triangle inequalities of the $3j-$symbols provide the following constraints:

$$\begin{aligned}
m_1 + m_2 &= M = \mu_1 + \mu_2 \\
&\max(|l_1 - l_2|, |\lambda_1 - \lambda_2|) \\
&\leq L \leq \min(l_1 + l_2, \lambda_1 + \lambda_2) \,.
\end{aligned}$$

Note that the sum over L, M in the $3j$-symbols in Eq. (31) does not allow a factorisation of terms between l_1, m_1, l_2, m_2 and $\lambda_1, \mu_1, \lambda_2, \mu_2$. To condense our expression a little we will use the abbreviation $\hat{x} \equiv 2x + 1$ to end up with

$$\begin{aligned}
\mathscr{Y}_{LM}(l_1, l_2, l_1', l_2') &= \langle (l_1 l_2) LM | \mathscr{Y}_4 | (l_1' l_2') LM \rangle \\
&= \sum_{\substack{m_1, m_2 \\ m_1', m_2'}} \langle l_1 m_1; l_2 m_2 | LM \rangle \mathscr{Y}_4 \\
&\quad (l_1, m_1, l_2, m_2, l_1', m_1', l_2', m_2') \langle l_1' m_1'; l_2' m_2' | LM \rangle \\
&= \frac{1}{4\pi} \sqrt{\hat{l}_1 \hat{l}_2 \hat{l}_1' \hat{l}_2'} \sum_{\mathscr{L}\mathscr{M}} \hat{\mathscr{L}} \begin{pmatrix} l_1 & l_2 & \mathscr{L} \\ 0 & 0 & 0 \end{pmatrix} \begin{pmatrix} l_1' & l_2' & \mathscr{L} \\ 0 & 0 & 0 \end{pmatrix} \\
&\quad \sum_{m_1 m_2} \langle l_1 m_1; l_2 m_2 | LM \rangle \begin{pmatrix} l_1 & l_2 & \mathscr{L} \\ -m_1 & -m_2 & \mathscr{M} \end{pmatrix} \\
&\quad \sum_{m_1' m_2'} \langle l_1' m_1'; l_2' m_2' | LM \rangle \begin{pmatrix} l_1' & l_2' & \mathscr{L} \\ m_1' & m_2' & -\mathscr{M} \end{pmatrix} .
\end{aligned} \tag{32}$$

We substituted $\mathscr{Y}_4(l_1, m_1, l_2, m_2, l_1', m_1', l_2', m_2')$ with Eq. (31) (and used the invariance of the $3j$-symbols under cyclic permutation of indices). We further express the $3j$-symbols using Clebsch–Gordan coefficients,

$$\begin{pmatrix} l_1 & l_2 & \mathscr{L} \\ -m_1 & -m_2 & \mathscr{M} \end{pmatrix} = \frac{(-1)^{l_1 - l_2 - \mathscr{M}}}{\sqrt{\hat{\mathscr{L}}}} \langle l_1, -m_1; l_2, -m_2 | \mathscr{L}, \mathscr{M} \rangle, \tag{33}$$

$$\begin{pmatrix} l_1' & l_2' & \mathscr{L} \\ m_1' & m_2' & -\mathscr{M} \end{pmatrix} = \frac{(-1)^{l_1' - l_2' + \mathscr{M}}}{\sqrt{\hat{\mathscr{L}}}} \langle l_1', m_1'; l_2', m_2' | \mathscr{L}, -\mathscr{M} \rangle. \tag{34}$$

Summing over the magnetic quantum numbers m_1' and m_2 and applying the orthogonality of Clebsch–Gordan coefficients, the sum collapses to two Kronecker Deltas,

$$\begin{aligned}
&\sum_{m_1' m_2'} \langle l_1' m_1'; l_2' m_2' | LM \rangle \langle l_1', m_1'; l_2', m_2' | \mathscr{L}, -\mathscr{M} \rangle \\
&\qquad = \delta_{L,\mathscr{L}} \delta_{M,-\mathscr{M}} \,.
\end{aligned} \tag{35}$$

Equation (32) therefore becomes

$$\begin{aligned}
\mathscr{Y}_{LM}(l_1, l_2, l_1', l_2') = (-1)^{l_1 - l_2 + l_1' - l_2'} &\frac{1}{4\pi} \sqrt{\hat{l}_1 \hat{l}_2 \hat{l}_1' \hat{l}_2'} \\
&\times \begin{pmatrix} l_1 & l_2 & L \\ 0 & 0 & 0 \end{pmatrix} \begin{pmatrix} l_1' & l_2' & L \\ 0 & 0 & 0 \end{pmatrix} \\
&\times \sum_{m_1 m_2} \langle l_1 m_1; l_2 m_2 | LM \rangle \\
&\langle l_1, -m_1; l_2, -m_2 | L, -M \rangle
\end{aligned} \tag{36}$$

Now we use the property

$$\begin{aligned}
&\langle l_1, -m_1; l_2, -m_2 | L, -M \rangle \\
&\qquad = (-1)^{l_1 - l_2 - L} \langle l_1, m_1; l_2, m_2 | L, M \rangle,
\end{aligned}$$

and the remaining sums over m_1 and m_2 give unity, leading to the final expression

$$\begin{aligned}
\mathscr{Y}_{LM}(l_1, l_2, l_1', l_2') \;= (-1)^{l_1' - l_2' - L} &\frac{1}{4\pi} \sqrt{\hat{l}_1 \hat{l}_2 \hat{l}_1' \hat{l}_2'} \\
&\begin{pmatrix} l_1 & l_2 & L \\ 0 & 0 & 0 \end{pmatrix} \begin{pmatrix} l_1' & l_2' & L \\ 0 & 0 & 0 \end{pmatrix}
\end{aligned}$$

$$= \frac{1}{4\pi}\sqrt{\hat{l}_1\hat{l}_2\hat{l}'_1\hat{l}'_2}\begin{pmatrix} l_1 & l_2 & L \\ 0 & 0 & 0 \end{pmatrix}\begin{pmatrix} l'_1 & l'_2 & L \\ 0 & 0 & 0 \end{pmatrix}, \tag{37}$$

where we used the fact that for non-vanishing $3j$ coefficient, $l'_1 + l'_2 + L =$ must be even, which implies that the factor

$$(-1)^{l'_1 - l'_2 - L} = 1. \tag{38}$$

Inserting this result in Eq. (30) leaves us with the final form of the matrix element,

$$\begin{aligned}\langle (l_1 l_2) LM|\hat{V}_{12}|(l'_1 l'_2) LM\rangle &= \frac{C(\Lambda)}{R^2}\sum_{\substack{m_1, m_2 \\ m'_1, m'_2}} \langle l_1 m_1; l_2 m_2|LM\rangle \\ &\quad \times \mathscr{Y}_4(l_1, m_1, l_2, m_2, l'_1, m'_1, l'_2, m'_2) \\ &\quad \times \langle l'_1 m'_1; l'_2 m'_2|LM\rangle \\ &\equiv \frac{C(\Lambda)}{R^2}\mathscr{Y}_{LM}(l_1, l_2, l'_1, l'_2). \end{aligned} \tag{39}$$

Note that the sums are restricted such that $m_1 + m_2 = M = m'_1 + m'_2$. The matrix element $\mathscr{Y}_{LM}(l_1, l_2, l'_1, l'_2)$ can be analytically determined and is separable,

$$\begin{aligned}\mathscr{Y}_{LM}(l_1, l_2, l'_1, l'_2) = \frac{1}{4\pi}&\left[\sqrt{(2l_1+1)(2l_2+1)}\begin{pmatrix} l_1 & l_2 & L \\ 0 & 0 & 0 \end{pmatrix}\right] \\ &\times\left[\sqrt{(2l'_1+1)(2l'_2+1)}\begin{pmatrix} l'_1 & l'_2 & L \\ 0 & 0 & 0 \end{pmatrix}\right] \end{aligned} \tag{40}$$

This last relation, combined with Eq. (39), gives the stated result in Eq. (8).

References

1. J.M. Alarcón et al., Neutron-proton scattering at next-to-next-to-leading order in nuclear lattice effective field theory. Eur. Phys. J. A **53**(5), 83 (2017). https://doi.org/10.1140/epja/i2017-12273-x. arXiv: 1702.05319 [nucl-th]
2. S.R. Beane et al., Two nucleons on a lattice. Phys. Lett. B **585**, 106–114 (2004). https://doi.org/10.1016/j.physletb.2004.02.007. arXiv: hep-lat/0312004
3. S.R. Beane, Ground state energy of the interacting Bose gas in two dimensions: an explicit construction. Phys. Rev. A **82**, 063610 (2010). https://doi.org/10.1103/PhysRevA.82.063610. arXiv: 1002.3815 [cond-mat.quant-gas]
4. R.A. Briceno, Z. Davoudi, T.C. Luu, Two-nucleon systems in a finite volume: (I) quantization conditions. Phys. Rev. D **88.3**, 034502 (2013). https://doi.org/10.1103/PhysRevD.88.034502. arXiv: 1305.4903 [hep-lat]
5. R.A. Briceño et al., Two-nucleon systems in a finite volume. II. 3S1-3 D1 coupled channels and the deuteron. Phys. Rev. D **88.11**, 114507 (2013). https://doi.org/10.1103/PhysRevD.88.114507. arXiv: 1309. 3556 [hep-lat]
6. T. Busch et al., Two cold atoms in a harmonic trap. Foundations Phys. **28**, 549–559 (1998). https://doi.org/10.1023/A:1018705520999
7. M.A. Caprio, P. Maris, J.P. Vary, Halo nuclei 6He and 8He with the Coulomb–Sturmian basis. Phys. Rev. C **90**(3), 034305 (2014). https://doi.org/10.1103/PhysRevC.90.034305. (**1409.0877 [nucl-th]**)
8. K.A. Dawson, Two particles on a sphere. J. Chem. Phys. **83**(9), 4822 (1985). https://doi.org/10.1063/1.449011
9. P. Egelhof et al., Nuclear-matter distributions of halo nuclei from elastic proton scattering in inverse kinematics. Eur. Phys. J. A **15**(1), 27–33 (2002). https://doi.org/10.1140/epja/i2001-10219-7
10. A.R. Edmonds. *Angular Momentum in Quantum Mechanics. Investigations in Physics Series* (Princeton University Press, Princeton, 1996). ISBN: 9780691025896. https://books.google.de/books?id=0BSOg0oHhZ0C
11. G.S. Ezra, R.S. Berry, Correlation of two particles on a sphere. Phys. Rev. A **25**, 1513–1527 (1982). https://doi.org/10.1103/PhysRevA.25.1513
12. G.S. Ezra, R.S. Berry, Collective and independent-particle motion in doubly excited two electron atoms. Phys. Rev. A **28**, 1974–1988 (1983). https://doi.org/10.1103/PhysRevA.28.1974
13. K. Fossez, J. Rotureau, W. Nazarewicz, Energy spectrum of neutron-rich helium isotopes: complex made simple. Phys. Rev. C **98**, 061302 (2018). https://doi.org/10.1103/PhysRevC.98.061302
14. H.-W. Hammer, C. Ji, D.R. Phillips, Effective field theory description of halo nuclei. J. Phys. G **44**(10), 103002 (2017). https://doi.org/10.1088/1361-6471/aa83db. arXiv: 1702.08605 [nucl-th]
15. H.-W. Hammer, S. König, U. van Kolck, Nuclear effective field theory: status and perspectives. Rev. Mod. Phys. **92.2**, 025004 (2020). https://doi.org/10.1103/RevModPhys.92.025004. arXiv: 1906.12122 [nucl-th]
16. H.. -W. Hammer, D. Lee, Causality and the effective range expansion. Ann. Phys. **325**, 2212–2233 (2010). https://doi.org/10.1016/j.aop.2010.06.006. arXiv: 1002.4603 [nucl-th]
17. M. Hongo, D.T. Son, *Universal Properties of Weakly Bound Two-Neutron Halo Nuclei* (2022). arXiv: 2201.09912 [nucl-th]
18. J.H. Kelley et al., Energy levels of light nuclei. Nucl. Phys. A **880**, 88–195 (2012). https://doi.org/10.1016/j.nuclphysa.2012.01.010
19. T. Kohler, K. Goral, P.S. Julienne, Production of cold molecules via magnetically tunable Feshbach resonances. Rev. Mod. Phys. **78**, 1311–1361 (2006). https://doi.org/10.1103/RevModPhys.78.1311. arXiv: cond-mat/0601420
20. C. Körber, E. Berkowitz, and T. Luu. *Renormalization of a Contact Interaction on a Lattice* (2019). arXiv: 1912.04425 [hep-lat]
21. T.A. Lähde, U.-G. Meißner, *Nuclear Lattice Effective Field Theory: An Introduction*, vol. 957 (Springer, Berlin, 2019). (**ISBN: 978-3-030-14187-5**)
22. B.-N. Lu et al., Precise determination of lattice phase shifts and mixing angles. Phys. Lett. B **760**, 309–313 (2016). https://doi.org/10.1016/j.physletb.2016.06.081. arXiv: 1506.05652 [nucl-th]
23. M. Lüscher, Volume dependence of the energy spectrum in massive quantum field theories. 2. Scattering states. Commun. Math. Phys. **105**, 153–188 (1986). https://doi.org/10.1007/BF01211097
24. M. Lüscher, Two particle states on a torus and their relation to the scattering matrix. Nucl. Phys. B **354**, 531–578 (1991). https://doi.org/10.1016/0550-3213(91)90366-6
25. T. Luu, M.J. Savage, Extracting scattering phase-shifts in higher partial-waves from lattice QCD calculations. Phys. Rev. D **83**, 114508 (2011). https://doi.org/10.1103/PhysRevD.83.114508. arXiv: 1101.3347 [hep-lat]
26. T. Luu et al., Nucleon–nucleon scattering in a harmonic potential. Phys. Rev. C **82**, 034003 (2010). https://doi.org/10.1103/PhysRevC.82.034003. arXiv: 1006.0427 [nucl-th]
27. V.V. Pupyshev, The length and effective radius of two dimensional scattering of a quantum particle by a centrally symmetric short-range potential. Theor. Math. Phys. **180**(3), 1051–1072 (2014). https://doi.org/10.1007/s11232-014-0199-1

28. M. Seidl, Adiabatic connection in density-functional theory: two electrons on the surface of a sphere. Phys. Rev. A **75**, 062506 (2007). https://doi.org/10.1103/PhysRevA.75.062506
29. M. Smith et al., First penning-trap mass measurement of the exotic halo nucleus 11Li. Phys. Rev. Lett. **101**, 202501 (2008). https://doi.org/10.1103/PhysRevLett.101.202501
30. I. Tanihata et al., Measurements of interaction cross- sections and nuclear radii in the light p shell region. Phys. Rev. Lett. **55**, 2676–2679 (1985). https://doi.org/10.1103/PhysRevLett.55.2676
31. D.R. Tilley et al., Energy levels of light nuclei A=5, A=6, A=7. Nucl. Phys. A **708**, 3–163 (2002). https://doi.org/10.1016/S0375-9474(02)00597-3
32. M.V. Zhukov et al., Bound state properties of Borromean Halo nuclei: He-6 and Li-11. Phys. Rept. **231**, 151–199 (1993). https://doi.org/10.1016/0370-1573(93)90141-Y